HHS Public Access

Author manuscript

Biomaterials. Author manuscript; available in PMC 2016 October 01.

Published in final edited form as:

Biomaterials. 2015 October ; 65: 175–183. doi:10.1016/j.biomaterials.2015.06.045.

An *In Vivo* Study of a Gold Nanocomposite Biomaterial for Vascular Repair

Allison M. Ostdiek, DVM, PhD,
Department of Veterinary Pathobiology, University of Missouri, Columbia, MO 65211, USA

Jan R. Ivey,
Department of Biomedical Sciences, University of Missouri, Columbia, MO 65211, USA

David A. Grant,
Department of Bioengineering, University of Missouri, Columbia, MO 65211, USA

Raja Gopaldas, MD, and
Prairie Cardiovascular, Springfield, IL 62701 USA

Sheila A. Grant, PhD
250 Agricultural Engineering, Columbia, Missouri 65211, USA, TEL: 1-573-884-9666, FAX: 1-573-882-1115

Allison M. Ostdiek: amostdiek@gmail.com; Jan R. Ivey: iveyj@missouri.edu; David A. Grant: grantdav@missouri.edu; Raja Gopaldas: rgopaldas@icloud.com; Sheila A. Grant: grantsa@missouri.edu

Abstract

Currently vascular repairs are treated using synthetic or biologic patches, however these patches have an array of complications, including calcification, rupture, re-stenosis, and intimal hyperplasia. An active patch material composed of decellulzarized tissue conjugated to gold nanoparticles (AuNPs) was developed and the long term biocompatibility and cellular integration was investigated. Porcine abdominal aortic tissue was decellularized and conjugated with 100nm gold nanoparticles (AuNP). These patches were placed over a longitudinal arteriotomy of the thoracic aorta in six pigs. The animals were monitored for six months. Gross, histological, and immunohistochemical analyses of the patches were performed after euthanasia. Grossly there was minimal scar tissue with the patches still visible on the outer surface of the vessel. The inner lumen was smooth with a seamless transition from patch to native tissue. Histology demonstrated infiltration of host cells into the patch material. The immunohistochemical results demonstrated an endothelial cell layer forming over the patch within the vessel. Smooth muscle cells were repopulating the biomaterial in all animals. These results demonstrated that the AuNP biomaterial patch integrated well with the host tissue and did not failed over the six month implantation time.

Correspondence to: Sheila A. Grant, grantsa@missouri.edu.

Keywords

Vascular patch; gold nanoparticles; decellularized tissue; biomaterials

1. Introduction

Vascular patch materials are used to repair and reconstruct damage to blood vessels [1–3]. These patch materials ideally mimic the native extracellular matrix, sustain and guide new cell growth, avoid intimal hyperplasia, resist infection, and degrade after new tissue has formed [4–9]. Unfortunately an ideal material has not yet been created, and thus a variety of synthetic and biologic materials are being investigated [10, 11]. The currently used synthetic and biological materials can cause immune reactions, infections, calcification, and neo-intimal hyperplasia [3, 12–16].

Synthetic materials such as expanded polytetrafluoroethylene are strong and long lasting *in vivo*. However they are susceptible to thrombus formation, calcification, and infection [17]. The native tissue tends to have a strong foreign body response to these types of materials and this can lead to chronic inflammation. The cells have difficulty integrating into these synthetic materials which in turn leads to their inability to continue growing when used in pediatric patients [18]. Biologic materials such as bovine pericardium and small intestine submucosa (SIS) better approximate characteristics of the native tissue than synthetic materials, but tend to be weaker and degrade quicker in the body [19, 20] if not crosslinked. Both types of materials may present foreign body responses, intimal hyperplasia and/or increased thrombogenicity when compared to native tissue [21].

To mitigate these problems, new types of materials and surface modifications are being explored. Biomimetic materials that possess cell-specific adhesion sites (such as RGD) and/or deliver bioactive factors such the drug dipyridamole have been investigated to improve cardiac function and prevent graft occlusion [22]. Numerous studies have investigated mechanical stiffness and methods to modulate the stiffness to reduce hyperplasia while electrical conductivity has been investigated to encourage cellular ingrowth into the vascular grafts. A group of researchers have also investigate plasma treatments for improving cell biocompatibility in a biodegradable polymer vascular graft [23]. The group electrospun poly(e-caprolactone) (PCL) to create nano-fiber scaffolds and then treated the scaffolds to air plasma using a radiofrequency plasma chamber to increase surface hydrophilicity. The results demonstrated improved neo-tissue formation in vivo. A variety of electrospun scaffolds for tissue engineering of vascular grafts have been investigated in order to better mimic the mechanical properties of blood vessels [24].

One type of modification that shows promise is the attachment of gold nanoparticles (AuNPs) to synthetic materials and acellular tissue. AuNPs have advantageous properties that make them a possible candidate to improve overall biocompatibility. For example, AuNPs are biologically inert and have been shown to increase resistance to bacterial adhesions; AuNPs have also been shown to aid fibroblast cell proliferation [25–29]. AuNPs conjugated to poly(ether)urethane polymers have been shown to improve the thermal and mechanical properties of materials [25] while AuNP conjugated to acellular tissue creates a

more stable construct [30]. For example, 100 nm AuNPs conjugated to Type I collagen was found to improve the resistance to collagenase resulting in as little as 7% degradation as compare to 100% degradation in non-AuNP collagen construct [30]. AuNPs conjugated to acellular tissue also delayed degradation while maintaining similar mechanical properties of the native tissue [31]. The use of AuNPs are being investigated in numerous medical applications such as drug delivery, imaging, biosensors, diagnostics, gene therapy, and nanocomposite biomaterials due to their biocompatibility, optical properties, and conjugation capabilities [32–36].

In this study, we developed a nanocomposite vascular patch by conjugating gold nanoparticles to decellularized arterial tissue matrices and performed a preliminary, long term *in vivo* test of our patch material. Our objectives were to 1) better match mechanical properties and structure by replacing a blood vessel with an acellular blood vessel patch and 2) improve tissue remodeling via the utilization of gold nanoparticles conjugated to an acellular blood vessel patch. It was hypothesized that the AuNP-acellular patch would show minimal immune response, endothelial and smooth muscle cell regeneration, and overall integration and biocompatibility with the host tissue. The AuNP-acellular patches were implanted on the thoracic aorta of swine. Six months after implantation, wound healing, tissue remodeling, endothelial cell regeneration, and cellular integration were investigated by gross, histological, immunohistochemical, and electron microscopic analyses. We are one of the first groups to synthesize, characterize, and perform a long-term *in vivo* study on a nanocomposite vascular patch.

2. Materials and methods

2.1 Tissue Harvest and Decellularization

Decellularization was performed following a previously published protocol [37, 38]. Porcine abdominal aortas were harvested immediately following euthanasia of swine at the University of Missouri. Blood and any excess connective tissue were removed and then they were immersed in distilled water for 24 hours at 4° C. The vessels were treated with 0.025% trypsin EDTA (ATCC) diluted in Dulbecco's phosphate buffered saline (dPBS; ATCC) for 24 hours at 37 °C. The tissue was decellularized with a solution of 1% Triton x-100 (Sigma) and 0.1% ammonium hydroxide (Fisher) in distilled water for 72 hours at 4 °C. It was then washed in a solution of Eagle's Minimum Essential Medium (EMEM; ATCC) 10% (v/v) horse serum and PennStrep (200 U/mL). The material was immersed for 24 hours in distilled water at 4 °C and then for 48 hours in PBS at 4 °C, changing the PBS to fresh solution at 24 hours. All of these steps were done with agitation.

2.2 Crosslinking

Decellularized patches were incubated for 15 minutes at ambient temperature in a crosslinking solution (50:50 (v/v) solution of acetone and PBS with 1-ethyl-3-[3-dimethylaminopropyl]carbodiimide (EDC) and *N*-hydroxysuccinimide(NHS). 100 nm AuNPs at 4 times the stock solution were functionalized using a solution of 2-mercaptoethylamine and added to the tissue. The 100 nm AuNPs were utilized due to a previous study demonstrating the viability of the 100 nm AuNPs [39]. The patches were

incubated for 24 hours at ambient temperature with gentle agitation followed by two 24 hour PBS rinses. Sterilization occurred via immersion in an aqueous solution of 0.1%(v/v) peracetic acid with 1.0M NaCl for 30 minutes followed by two 24 hour sterile PBS rinses at ambient temperature with shaking.

2.3 Mechanical and Suture Pullout Testing

Suture pullout testing was performed on native porcine aortic tissue (n=5), decellularized porcine aortic tissue (n=7), crosslinked porcine aortic tissue (n=9), and bovine pericardium (n=5). The bovine pericardium was chosen to represent the typical biologic repair patch that would be used in human medicine. Previous work has shown that the addition of AuNPs did not significantly change the mechanical properties of the material, so they were not retested here [31]. Each piece of tissue was cut into a 10mm × 10mm strip. A piece of 6-0 prolene suture that is typically used for this type of procedure *in vivo* was tied 3mm from one edge to create a 5mm loop. The tissue was gripped with a pneumatic grip set to 52psi, and the suture was placed over an opposing hook. An Instron TA.XT2 mechanical testing system (Texture Technologies, Corporation, Scarsdale, NY) was utilized to strain the specimens at a rate of 0.2mm/s until failure. If the suture broke before pulling out of the tissue the test results were discarded. The tensile strength at yield was calculated by dividing the maximum load, Fmax, by the original cross-sectional area, A, of the specimen. The modulus of elasticity E, was determined from the slope of a line fit to the stress versus strain curve of each specimen.

2.4 Implantation

Female domestic swine (n=6) with a starting weight of approximately 120 lbs were housed in accordance with the *Guide for the Care and Use of Laboratory Animals* under a protocol approved by the Institutional Animal Care and Use Committee. Twenty-four hours before surgery animals were given 325 mg aspirin orally (PO). Intramuscular (IM) telazol (4.4–6.6 mg/kg body weight), xylazine (2.2 mg/kg) and atropine (0.05 mg/kg) were given as a preanesthetic. 2–4% Isoflurane was administered via nose cone until the animal was sedated enough to be safely intubated. A surgical plane of anesthesia was maintained using 1–3% isoflurane gas and a ventilator at 6–8 breaths/minute. Prior to the incision animals were given ceftiofur (5 mg/kg IM). An intravenous (IV) catheter was placed in the ear with an isotonic sodium chloride flow throughout surgery. Heparin was given IV at an initial bolus of 10,000 U/kg followed by 5,000 u/kg every hour intra op when necessary. Pancuronium (0.1 mg/kg IV) was given at the time of the incision.

The aorta was reached through the fourth rib space via a left lateral thoracotomy. The aorta was partially clamped and opened in the longitudinal direction. Patch material was sutured over the defect using 6-0 prolene.

After patch placement, Doppler ultrasound (LS probe on a Logique GE ultrasound) was used to visualize the flow through the arteries. Ultrasound was also performed at 6 months, prior to the conclusion of the study. Color flow and waveform characteristics were imaged and used to ensure patency. All vessels were patent immediately after surgery and prior to sacrifice at 6 months (results not shown).

Post operatively a 75 μg/hr fentanyl patch was placed on the dorsum for pain relief and carprofen (3mg/kg) subcutaneously (SQ) and buprenorphine (0.01–0.02 mg/kg) IM were given to bridge the gap until the fentanyl became effective. Animals received 325 mg aspirin PO for 3 days post op and then 81 mg/day PO until sacrifice.

2.5 Gross Examination

Each artery was photographed (Canon PowerShot A4000 IS) *in vivo* after the thorax of the animal had been re-opened. The lumen was photographed after the artery was explanted.

2.6 Histology

All slides were prepared by IDEXX Bioresearch (Columbia, MO). Samples were fixed in 10% (v/v) buffered formalin, dehydrated with a graded ethanol series, embedded in paraffin and cut to a thickness of 5 μm with a microtome. The histology slides were stained with hematoxylin and eosin (H&E), as well as van Gieson's method to look at elastin and collagen was stained for using Masson's trichrome. All slides were viewed at 50×, 100×, 200×, and 400× on a Zeiss Axiophot (Carl Zeiss Microimaging, Inc., Thornwood, NY) and photographs were acquired using an Olympus DP70 (Olympus America Inc., Center Valley, PA) camera with DP Manager Version 1.21.107 as the acquisition software.

2.7 Immunohistochemistry

All slides were prepared by IDEXX Bioresearch (Columbia, MO). Samples were fixed in 10% (v/v) buffered formalin, dehydrated with a graded ethanol series, embedded in paraffin and cut to a thickness of 5 μm with a microtome. The slides were deparaffinized using a standard protocol of xylene, to absolute alcohol, 95% alcohol to water. They were then immersed in 5% bovine serum albumin (Sigma A3294-50) for 20 minutes followed by CD31 (Abcam ab28364) at a 1:50 ratio for one hour. They were rinsed using a Dako wash buffer (Dako K1492). Next the slides were submerged in the goat anti-rabbit IgG Alexafluor 594 red (Invitrogen A11037) at a 1:500 ratio for 30 minutes followed by another Dako rinse and then put in bovine serum albumin for 20 minutes. They were dyed with Actin Smooth Muscle (Dako M0851) at a 1:400 ratio for an hour, rinsed, and immersed in goat anti-mouse IgG Alexafluor 288 green (Molecular Probes A11001). Slides were rinsed again in Dako, then a coverslip with MoWiol(polyvinyl alcohol mounting medium with DABCO antifade - Fluka Cat #10981) was applied. They were viewed on a Leica TCP SP8 MP Inverted spectral confocal microscope with tunable white light laser at the University of Missouri Cytology Core. Images were taken using Leica software.

2.8 Statistical Analysis

GraphPad Prism v4.0 (GraphPad Software, Inc., San Diego, CA) was used to analyze experimental data. One-way analysis of variance (ANOVA) with a 95% confidence interval was conducted followed by a Tukey-Kramer post-test to determine significant differences between means of the experimental groups for the mechanical testing and biocompatibility assays. Values are reported and graphed as the mean ± standard error of the mean.

3. Results

3.1 Mechanical and Suture Pullout Testing

The suture pullout tests demonstrated that the bovine pericardial patch had a significantly higher Modulus of Elasticity and Tensile Stress at the maximum load when compared to other three groups of the porcine tissue. The results of the modulus of elasticity and the tensile stress at maximum load are graphed in Figures 1a and 1b respectively. The modified porcine tissue was not significantly different in mechanical properties from the porcine native aorta or the porcine decellularized aorta.

3.2 Implantation

Overall, implantation went smoothly for 5 of the 6 animals. The sixth animal was awakening from the anesthetic when she experienced a cardiac event and could not be revived. The thoracic cavity was reopened and the patch was still in place and not the cause of death. A portion of the aorta along with the patch was harvested and used as baseline controls. All other animals survived to their time point of 6 months. Figure 2 shows the approach, isolation, and implantation of the patch into the aorta.

3.3 Gross Examination

After 6 months the aortas were removed from the animals. Upon approach minimal scar tissue was seen within the thoracic cavity of most of the animals as shown in Figure 3. The patch integrated smoothly on the luminal side with the native tissue. A decrease in the cross-sectional area of the lumen was not noted distal or proximal to the patch, indicating the absence of intimal hyperplasia.

3.4 Histology

Figure 4a displays the patch before the decellularization process and the nuclei of the cells are clearly visible. After decellularization it is apparent that the nuclear remnants have been removed (Figure 4b–d). Masson’s trichrome staining and van Gieson’s staining highlight the elastin and collagen tissue present in the extracellular matrix after decellularization. Figure 4e displays the presence of gold nanoparticles on the material after sterilization and before implantation.

After six months the explanted patch material demonstrated cellular integration, though there is still a noted boundary between the biomaterial and the native tissue. H&E staining as shown in Figure 4f demonstrated that the cells have infiltrated into the patch material, but no major congregation of immune cells, inflammatory cells, or signs of infection or fibrosis around the patch was noted in all five samples. As indicated in Figure 4g, trichrome staining demonstrated that the patch had a higher amount of collagen when compared to the native tissue while smooth muscle cell integration was noted via red staining. The van Gieson’s stain as shown in Figure 4h demonstrated that the patch stains less for elastin than the native tissue. The arrow in Figure 4h points to a transition zone though, where it appears the patch is becoming more similar to the native tissue.

3.5 Immunohistochemistry

Immunohistochemical analysis demonstrated that the cells present on the lumen side of the patches stained positively for CD31 (red fluorescence labeled) which indicated endothelial cell regeneration as shown in Figure 5b. The vessel had repaired the area over the patch and demonstrated a comparable endothelial cell layer as to the control animal's native vessel which is noted in Figure 5a. In Figures 5a and 5b, the green fluorescence labeled SM actin stain demonstrated that smooth muscle cells (SMCs) have re-populated the graft. As a comparison, Figure 5d displays the patch just after implantation (i.e., non-survival animal graft; approximately 2 hours in vivo) and highlights the gross differences in cellular integration that occurred after 6 months implantation. In Figure 5a and 5b respectively the native vessel is compared to the graft vessel. Figure 5c demonstrates the transition zone between the native tissue and the graft, highlighting while there are still some differences in the smooth muscle cell orientation, the cells are rebuilding within the extracellular matrix of the graft.

4. Discussion

A more intelligently engineered biomaterial could mitigate the negative aspects associated with the currently available biologic and synthetic vascular patch materials, and in recent years there have been innovative approaches to engineer resorbable biomaterials to induce sequential regeneration of the vascular wall and to achieve efficient re-endothelialization. These approaches have involved biomaterials that utilize both chemical [40–42] and topographical modifications [43, 44] to regulate smooth muscle cells (SMCs) over-proliferation and enhance ECM synthesis as well as other innovative biomaterials that are impregnated with stem cells and/or utilize biomechanical stimulation to improve overall biocompatibility [41, 45].

In a recent study, a collagen hydrogel construct doped with S-Nitrosoglutathione (GSNO) released exogenous nitric oxide in order to manipulate cell proliferation and matrix deposition by adult human aortic SMCs [40]. Growth factors such as transforming growth factor (TGF-β1) have also been conjugated to fibrin hydrogel vascular grafts and exposed to mechanical stimulation [41] to improve mechanical properties and ECM content. Mechanical stimulation has also been combined with mesenchymal stem cells (MSCs) cultured on micropatterned poly(e-caprolactone) films for improved functionally of SMCs [45]. Another study electrospun a larger pore and thicker polycaprolactone (PCL) fiber to construct vascular grafts that demonstrated immunomodulatory properties resulting in vascular regeneration [43]. Re-endothelialization was also achieved in a drug-eluting vascular graft design where the drug, simvastatin, was entrapped in a Thai silk fibroin/gelation-hydrogel graft. Simvastatin had promotional effects on endothelial progenitor cell (EPC) resulting in faster re-endothelialization [42].

In this paper, our approach was the utilization of decellularized arterial tissue which has similar mechanical properties and structure as the native vessels and thus could result in improved performance of vascular patches. In addition, the utilization of AuNPs may also extend the structural lifetime of the graft allowing for cellular infiltration and tissue regeneration. Mechanical studies were performed and the new material patch was compared

to a commercially available biological pericardium patch. The new patch was then subjected to a long term *in vivo* study to determine the native tissue interaction.

It is well-documented that differences in mechanical properties such as compliance between graft materials and native host tissue can lead to poor patency and anastomotic intimal hyperplasia [24, 46]. It was demonstrated by Sarkar et al. [47] that compliance mismatch between a graft and native vessel leads to unnatural wall shear stress which then results in poor graft patency. Also, a study performed in canines demonstrated that stiffer, high crosslinked vascular grafts led to more occlusion than less stiff (less crosslinked) grafts [48]. In another study, Wang et al. demonstrated that more compliant grafts match mechanical and flow parameters better than less compliant materials [49]. Our mechanical data demonstrated no significant difference in our patch materials and the native vessel, indicating similar compliance. However, there were significant differences in mechanical properties between the native porcine aortic tissue and the bovine pericardium, which is a commonly utilized patch material. The bovine pericardium showed a higher strength before failing, but was significantly stiffer than the porcine tissue. Stronger patch materials were thought to be necessary in order to withstand the *in vivo* arterial pressure. However, as shown by this study, our patch materials demonstrated the ability to withstand the blood pressure of the thoracic aorta as well as better matching of mechanical properties. This may explain why the patch material allowed for cellular integration and had no indications of thrombosis or intimal hyperplasia.

To determine the ability of the new patch to integrate with the host tissue without any adverse effect, a long term *in vivo* study was implemented. Overall, the implantation process of this material went smoothly, with the exception of one animal lost to anesthetic complications; the aorta was still intact at death with the patch still in place. During the 6 months, the animals were healthy and progressed well.

After explantation, the gross photos demonstrated minimal scar tissue in the chest, indicating the absence of any long-term chronic inflammatory response. The gross view of the lumen shows a smooth, well integrated patch. There were no thrombi seen, which can occur upon contact with foreign material [50]. Blood contact with polymeric synthetic materials typically will lead to adhesion and aggregation of platelets and a coagulation response; this response was not demonstrated with this patch material [51]. In addition, the graft remained patent with no evidence of intimal hyperplasia. Thrombus formation and intimal hyperplasia is a concern for many small diameter grafts and new, innovative techniques are being investigated. For example, an electrospun biodegrade elastic polyurethane small diameter vascular scaffold was investigated that would release an anti-coagulation drug, dipyridamole, over time. The results demonstrated steady release rates over time along with good patency of the graft [23].

While unique surface structures and bioactive factors can be added to synthetic materials, the utilization of the extracellular matrix (ECM) as a tissue construct has shown much promise. The benefits of leveraging the ECM to promote constructive remodeling through the natural release of growth factors when the ECM degrades have been reviewed [52, 53]. To achieve constructive remodeling, it is critical that the decellularization process not only

remove native cells and nuclei remnant, but also maintain the integrity of the ECM and is not subjective to extensive crosslinking. The decellularized process utilized to fabricate the porcine aortic patches succeeded in maintaining the ECM while eliminating possible immune responsive elements as shown in Figure 4. The collagen and elastin present in the patch matrix provides an organized scaffold for cells to adhere and proliferate [54]. In addition, the AuNPs as shown in Figure 4e have been shown to increase stability, decrease inflammation, and slow down scaffold degradation as demonstrated in earlier *in vitro* studies [30, 31, 34, 55–57]. The lack of thrombosis and other inflammatory and immune reactions may indicate that the patches' surface modifications are aiding in the host integration process.

The histologic images indicated that while the patch is integrated with native cells, there are still structural differences between the native vessel and the patch. The trichrome and van Geison's stains demonstrated that the patch had more collagen and less elastin than the native tissue, but a transition zone was apparent where the patch appeared to be remodeling into structurally similar native tissue as shown in Figure 4. With the H&E staining there were no signs of infection. After 6 months, there were no signs of macrophages and/or multi-nucleated giant cells, which are common signs of a chronic, long-term inflammatory response [58]. Often when a vascular wall repairs itself there is a generalized thickening of the media due to over proliferation of smooth muscle cells known as intimal hyperplasia [59, 60]. On the histologic and gross images for this study there is no thickening of the intimal layer between the native tissue and the AuNP-patches. Intimal hyperplasia would be evident at six months if it is going to occur.

The results of the immunohistochemical staining were particularly promising. They show definitive evidence that the native vessel has begun to remodel into the patch. The CD31 stain highlighted the layer of endothelial cells that has covered the patch. It is not overly thickened and comparable to the control tissue. The presence of an endothelial cell layer is important as decreases in endothelial derived substances result in a decreased ability to regulate coagulation [61]. When compared to the patch that had only been briefly implanted, the six months patches had excellent integration of smooth muscle cells in the extracellular matrix. Smooth muscle cells can over proliferate during vascular repair; however, they must be present to properly rebuild the vessel as they also play a role in synthesizing extracellular matrix [62–65]. The immunohistochemical staining shows that the smooth muscle cells are infiltrating the patch in a pattern similar to the native tissue.

5. Conclusions

This long term study examined the potential of a nanobiocomposite biomaterial for vascular repair and blood contacting applications. The biomaterial patch did not rupture in any of the animals tested and the long term survival of five of the animals. The patches were able to withstand the pressure of the aorta while allowing for endothelial and smooth muscle cell re-growth. The host cell integration demonstrated during this study highlighted the potential of this patch to integrate and regenerate new tissue. The reaction of the body to the patch supported the hypothesis that there would be minimal inflammatory response, endothelial and smooth muscle cell regeneration, and overall integration and biocompatibility. However,

the study examined only a limited number of cohorts. Further studies with a larger sample size are needed in order to draw definitive conclusions. Additionally, future studies in diseased animal models would be beneficial to determine the performance of the patch biomaterial in a less than ideal environment.

Acknowledgments

This research was sponsored in part by the University of Missouri by NIH Grant T32RR007004**,** and the University of Missouri Departments Bioengineering and Surgery. The authors would like to thank Drs. Scott Korte, Erin O'Connor, Marcia Hart, Sarah Hansen, Mike Fink, and Beth Ahner for their anesthetic and surgical assistance. Dr. Cindy Besch-Williford, Jan Adair, and Jill Hansen at IDEXX Bioresearch ensured the success of all histological and immunohistochemical slide staining.

References

1. Muto A, Nishibe T, Darkik A. Patches for Carotid Artery Endarterectomy: Current Materials and Prospects. Journal of Vascular Surgery. 2009; 50:206–213. [PubMed: 19563972]
2. Li X, Jadlowiec C, Guo Y, Protack CD, Ziegler KR, Lu W, Yang C, Shu C, Dardik A. Pericardial Patch Angioplasty Heals via an Ephrin-B2 and CD34 Positive Cell Mediated Mechanism. PLOS One. 2012; 7:1–8.
3. Cho SW, Park HJ, Ryu JH, Kim SH, Kim YH, Choi CY, et al. Vascular patches tissue-engineered with autologous bone marrow-derived cells and decellularized tissue matrices. Biomaterials. 2005; 26:1915–1924. [PubMed: 15576165]
4. Bordenave L, Menu P, Baquey C. Developments towards tissue-engineered, small-diameter arterial substitutes. Expert review of medical devices. 2008; 5:337–347. [PubMed: 18452384]
5. Kamenskiy AV, Mactaggart JN, Pipinos II, Gupta PK, Dzenis YA. Hemodynamically motivated choice of patch angioplasty for the performance of carotid endarterectomy. Ann Biomed Eng. 2013; 41:263–278. [PubMed: 22923061]
6. Williams C, Xie AW, Emani S, Yamato M, Okano T, Emani S, Wong JY. A comparison of human smooth muscle and mesenchymal stem cells as potential cell sources for tissue-engineered vascular patches. Tissue Engineering Part A. 2012; 18:986–998. [PubMed: 22145703]
7. Kumar VA, Caves JM, Haller CA, Dai E, Liu L, Grainger S, Chaikof EL. Acellular vascular grafts generated from collagen and elastin analogs. Acta Biomater. 2013; 9:8067–8074. [PubMed: 23743129]
8. Meroux-Berger M, Queguiner I, Maciel TT, Ho A, Relaix F, Kempf H. Pathologic Calcification of Adult Vascular Smooth Muscle Cells Differs on Their Crest or MesodermalEmbryonic Origin. J Bone Mineral Res. 2011; 26:1543–1553.
9. Zwirner K, Thiel C, Thiel K, Morgalla MH, Konigsrainer A, Schenk M. Extracellular brain ammonia levels in association with arterial ammonia, intracranial pressure and the use of albumin dialysis devices in pigs with acute liver failure. Metab Brain Dis. 2010; 25:407–412. [PubMed: 21086032]
10. Robinson KA, Li J, Mathison M, Redkar A, Cui J, Chronos NAF, et al. Extracellular Matrix Scaffold for Cardiac Repair. Circulation. 2005; 112:I-135–I-43. [PubMed: 16159805]
11. Stickler P, DeVisscher G, Mesure L, Famaey N, Martin D, Campbell JH, Van Oosterwyck H, Meuris B, Flameng W. Cyclically stretching developing tissue in vivo enhances mechanical strength and organization of vascular grafts. Acta Biomater. 2010; 6:2448–2456. [PubMed: 20123137]
12. Collins MJ, Li X, Dardik A. Therapeutic strategies to combat neointimal hyperplasia in vascular grafts. Expert Rev Cardiovascu Ther. 2012; 10:635–647.
13. Lehr EJ, Rayat GR, Chiu B, Churchill T, McGann LE, Coe JY, Ross DB. Decellularization reduces immunogenicity of sheep pulmonary artery vascular patches. J Thorac Cardiovasc Surg. 2011; 141:1056–1062. [PubMed: 20637475]

14. Varcoe RL, Mikhail M, Guiffre AK, Pennings G, Vacaretti M, Hawthorne WJ, Fletcher JP, Medbury HJ. The role of the fibrocyte in intimal hyperplasia. J Thrombosis Haemostasis. 2006; 4:1125–1133.
15. Matsagas M, Bali C, Arnaoutoglou E, Papakostas J, Nassis C, Papadopoulos G, et al. Carotid Endarterectomy with Bovine Pericardium Patch Angioplasty: Mid-Term Results. Annals of vascular surgery. 2006; 20:614–619. [PubMed: 16799852]
16. Muto A, Nishibe T, Dardik H, Dardik A. Patches for carotid artery endarterectomy: Current materials and prospects. Journal of Vascular Surgery. 2009; 50:206–213. [PubMed: 19563972]
17. Mehta RI, Mukerjee AK, Patterson TD, Fishbein MC. Pathology of explanted polytetrafluoroethylene vascular grafts. Cardiovasc Pathol. 2011; 20:213–221. [PubMed: 20619685]
18. Li X, Guo Y, Ziegler KR, Model LS, Eghbalieh SDD, Brenes RA, et al. Current Usage and Future Directions for the Bovine Pericardial Patch. Annals of vascular surgery. 2011; 25:561–568. [PubMed: 21276709]
19. Bolland F, Korossis S, Wilshaw S-P, Ingham E, Fisher J, Kearney JN, et al. Development and characterisation of a full-thickness acellular porcine bladder matrix for tissue engineering. Biomaterials. 2007; 28:1061–1070. [PubMed: 17092557]
20. Neethling WML, Strange G, Firth L, Smit FE. Interactive CardioVascular Thoracic Surg. 2013; 2013:1–5.
21. Frost MC, Reynolds MM, Meyerhoff ME. Polymers incorporating nitric oxide releasing/generating substances for improved biocompatibility of blood-contacting medical devices. Biomaterials. 2005; 26:1685–1693. [PubMed: 15576142]
22. Punnakitikashem P, Truong D, Menon JU, Nguyen KT, Hong Y. Electrospun biodegradable elastic polyurethane scaffolds with dipyridamole release for small diameter vascular grafts. Acta biomaterialia. 2014; 10:4618–4628. [PubMed: 25110284]
23. Valence, Sd; Tille, J-C.; Chaabane, C.; Gurny, R.; Bochaton-Piallat, M-L.; Walpoth, BH., et al. Plasma treatment for improving cell biocompatibility of a biodegradable polymer scaffold for vascular graft applications. European Journal of Pharmaceutics and Biopharmaceutics. 2013; 85:78–86. [PubMed: 23958319]
24. Hasan A, Memic A, Annabi N, Hossain M, Paul A, Dokmeci MR, Dehghani F, Khademhosseini A. Electrospun scaffolds for tissue engineering of vascular grafts. Acta Biomater. 2014; 10:11–25. [PubMed: 23973391]
25. Hsu SH, Tang CM, Tseng HJ. Biocompatibility of poly(ether)urethane-gold nanocomposites. J Biomed Mater Res A. 2006; 79:759–770. [PubMed: 16871514]
26. Castaneda L, Valle J, Yang N, Pluskat S, Slowinska K. Collagen cross-linking with Au nanoparticles. Biomacromolecules. 2008; 9:3383–3388. [PubMed: 18959440]
27. Hsu, S-h; Tang, C-M.; Tseng, H-J. Gold nanoparticles induce surface morphological transformation in polyurethane and affect the cellular response. Biomacromolecules. 2007; 9:241–248. [PubMed: 18163574]
28. Rai A, Prabhune A, Perry CC. Antibiotic mediated synthesis of gold nanoparticles with potent antimicrobial activity and their application in antimicrobial coatings. Journal of Materials Chemistry. 2010; 20:6789–6798.
29. Qu Y, Lü X. Aqueous synthesis of gold nanoparticles and their cytotoxicity in human dermal fibroblasts–fetal. Biomedical Materials. 2009; 4:025007. [PubMed: 19258699]
30. Grant SA, Spradling CS, Grant DN, Fox DB, Jimenez L, Grant DA, et al. Assessment of the biocompatibility and stability of a gold nanoparticle collagen bioscaffold. J Biomed Mater Res A. 2014; 102(2):332–339. [PubMed: 23670910]
31. Deeken CR, SL, Bachman BJ, Ramshaw SA. Grant, Characterization of Bionanocomposite Scaffolds Comprised of Mercaptoethylamine-Functionalized Gold Nanoparticles Crosslinked to an Acellular Porcine Tendon. Journal of Materials Science: Materials in Medicine. 2012; 23(2):537–546. [PubMed: 22071985]
32. Freese C, Gibson MI, Klok H-A, Unger RE, Kirkpatrick CJ. Size-and coating-dependent uptake of polymer-coated gold nanoparticles in primary human dermal microvascular endothelial cells. Biomacromolecules. 2012; 13:1533–1543. [PubMed: 22512620]

33. Lim Z-ZJ, Li J-EJ, Ng C-T, Yung L-YL, Bay B-H. Gold nanoparticles in cancer therapy. Acta Pharmacologica Sinica. 2011; 32:983–990. [PubMed: 21743485]
34. Whelove OE, Cozad MJ, Lee BD, Sengupta S, Bachman SL, Ramshaw BJ, et al. Development and in vitro studies of a polyethylene terephthalate-gold nanoparticle scaffold for improved biocompatibility. Journal of biomedical materials research Part B, Applied biomaterials. 2011; 99:142–149.
35. Gu Y-J, Cheng J, Lin C-C, Lam YW, Cheng SH, Wong W-T. Nuclear penetration of surface functionalized gold nanoparticles. Toxicology and applied Pharmacology. 2009; 237:196–204. [PubMed: 19328820]
36. Everts M, Saini V, Leddon JL, Kok RJ, Stoff-Khalili M, Preuss MA, et al. Covalently linked Au nanoparticles to a viral vector: potential for combined photothermal and gene cancer therapy. Nano Letters. 2006; 6:587–591. [PubMed: 16608249]
37. Amiel GE, Komura M, Shapira O, Yoo JJ, Yazdani S, Berry J, et al. Engineering of blood vessels from acellular collagen matrices coated with human endothelial cells. Tissue Eng. 2006; 12:2355–2365. [PubMed: 16968175]
38. Williams C, Liao J, Joyce EM, Wang B, Leach JB, Sacks MS, et al. Altered structural and mechanical properties in decellularized rabbit carotid arteries. Acta Biomater. 2009; 5:993–1005. [PubMed: 19135421]
39. Ostdiek AM, Grant DA, Grant SA. Mechanical and in vitro characterization of decellularized porcine aortic tissue conjugated with gold nanoparticles as a vascular repair material. International Journal of Biomaterials. In press.
40. Simmers P, Gishto A, Vyavahare N, Kothapalli CR. Nitric oxide stimulates matrix synthesis and deposition by adult human aortic smooth muscle cells within three-dimensional cocultures. Tissue Eng Part A. 2015; 21:1455–1470. [PubMed: 25597545]
41. Liang M-S, Koobatian M, Lei P, Swartz DD, Andreadis ST. Differential and synergistic effects of mechanical stimulation and growth factor presentation on vascular wall function. Biomaterials. 2013; 34:7281–7291. [PubMed: 23810080]
42. Thitiwuthikiat P, Ii M, Saito T, Asahi M, Kanokpanont S, Tabata Y. A vascular patch prepared from thai silk fibroin and gelatin hydrogel incorporating simvastatin-micelles to recruit endothelial progenitor cells. Tissue Eng Part A. 2015; 21:1309–1319. [PubMed: 25517108]
43. Wang Z, Cui Y, Wang J, Yang X, Wu Y, Wang K, Gao X, Li D, Li Y, Zheng X-L, Zhu Y, Kong D, Zhao Q. The effect of thick fibers and large pores of electrospun poly(ε-caprolactone) vascular grafts on macrophage polarization and arterial regeneration. Biomaterials. 2014; 35:5700–5710. [PubMed: 24746961]
44. Sylvester A, Sivaraman B, Deb P, Ramamurthi A. Nanoparticles for localized delivery of hyaluronan oligomers towards regenerative repair of elastic matrix. Acta Biomaterialia. 2013; 9:9292–9302. [PubMed: 23917150]
45. Wang Z-Y, Teoh SH, Johana NB, Chong M, Teo EY, Hong M-H, Chan JK, Thian ES. Enhancing mesenchymal stem cell response using uniaxially stretched poly(3-caprolactone) film micropatterns for vascular tissue engineering application. Mater Chem B. 2014; 2:5898–5909.
46. Ghista DN, Kabinejadian F. Coronary artery bypass grafting hemodynamics and anastomosis design: A biomedical engineering review. Biomedical Engineering Online. 2013; 12:1–53. [PubMed: 23289769]
47. Sarkar S, Salacinski H, Hamilton G, Seifalian A. The mechanical properties of infrainguinal vascular bypass grafts: their role in influencing patency. European journal of vascular and endovascular surgery. 2006; 31:627–636. [PubMed: 16513376]
48. Abbott WM, Megerman J, Hasson JE, L'Italien G, Warnock DF. Effect of compliance mismatch on vascular graft patency. Journal of vascular surgery. 1987; 5:376–382. [PubMed: 3102762]
49. Wang X, Lin P, Yao Q, Chen C. Development of small-diameter vascular grafts. World J Surg. 2007; 31:682–689. [PubMed: 17345123]
50. Courtney J, Lamba N, Sundaram S, Forbes C. Biomaterials for blood-contacting applications. Biomaterials. 1994; 15:737–744. [PubMed: 7986936]

51. Fink H, Faxalv L, Molnar GR, Drotz K, Risberg B, Lindahl TL, Sellborn A. Real-time measurements of coagulation on bacterial cellulose and conventional vascular graft materials. Acta Biomater. 2010; 6:1125–1130. [PubMed: 19800035]
52. Badylak S, Freytes DO, Gilbert TW. Extracellular matrix as a biologica scaffold material: Structure and function. Acta Biomaterialia. 2009; 5:1–13. [PubMed: 18938117]
53. Badylak S, Brown BN, Gilbert TW, Daly KA, Huber A, Turner NJ. Biologic scaffolds for constructive tissue remodeling. Biomaterials. 2011; 32:316–319. [PubMed: 21125721]
54. Bader A, Steinhoff G, Strobl K, Schilling T, Brandes G, Mertsching H, et al. Engineering of human vascular aortic tissue based on a xenogeneic starter matrix. Transplantation. 2000; 70:7–14. [PubMed: 10919568]
55. Deeken CR, Fox DB, Bachman SL, Ramshaw BJ, Grant SA. Characterization of Bionanocomposite Scaffolds Comprised of Amine-Functionalized Gold Nanoparticles and Silicon Carbide Nanowires Crosslinked to an Acellular Porcine Tendon. Journal of Biomedical Materials Research B. 2011; 97B(2):334–344.
56. Deeken CR, Fox DB, Bachman SL, Ramshaw BJ, Grant SA. Assessment of the Biocompatibility of Two Novel, Bionanocomposite Scaffolds in a Rodent Model. Journal of Biomedical Materials Research B. 2011; 96B(2):351–359.
57. Grant DN, Benson J, Cozad MJ, Whelove OE, Bachman SL, Ramshaw BJ, Grant DA, Grant SA. Conjugation of Gold Nanoparticles to Polypropylene Mesh for Enhanced Biocompatibility. Journal of Materials Science: Materials in Medicine. 2011; 22(12):2803–2812. [PubMed: 21979166]
58. Velnar T, Bailey T, Smrkolj V. The wound healing process: an overview of the cellular and molecular mechanisms. Journal of International Medical Research. 2009; 37:1528–42. [PubMed: 19930861]
59. Glagov S, Zarins C, Giddens D, Ku DN. Hemodynamics and atherosclerosis. Insights and perspectives gained from studies of human arteries. Archives of pathology & laboratory medicine. 1988; 112:1018–31. [PubMed: 3052352]
60. Rodbard S. Negative feedback mechanisms in the architecture and function of the connective and cardiovascular tissues. Perspectives in biology and medicine. 1969; 13:507–27. [PubMed: 5474042]
61. Weber, KT. Vascular Wound Healing and Restenosis Following Revascularization. In: Weber, KT., editor. Wound Healing in Cardiovascular Disease. Armonk, NY: Futura Publishing Company; 1995. p. 137-47.
62. Thyberg J, Blomgren K, Roy J, Tran PK, Hedin U. Phenotypic modulation of smooth muscle cells after arterial injury is associated with changes in the distribution of laminin and fibronectin. Journal of Histochemistry & Cytochemistry. 1997; 45:837–46. [PubMed: 9199669]
63. Chamley-Campbell JH, Campbell GR. What controls smooth muscle phenotype? Atherosclerosis. 1981; 40:347–57. [PubMed: 7332614]
64. Campbell GR, Campbell JH. Smooth muscle phenotypic changes in arterial wall homeostasis: implications for the pathogenesis of atherosclerosis. Experimental and molecular pathology. 1985; 42:139–62. [PubMed: 3884359]
65. Newby AC, Zaltsman AB. Molecular mechanisms in intimal hyperplasia. The Journal of Pathology. 2000; 190:300–9. [PubMed: 10685064]

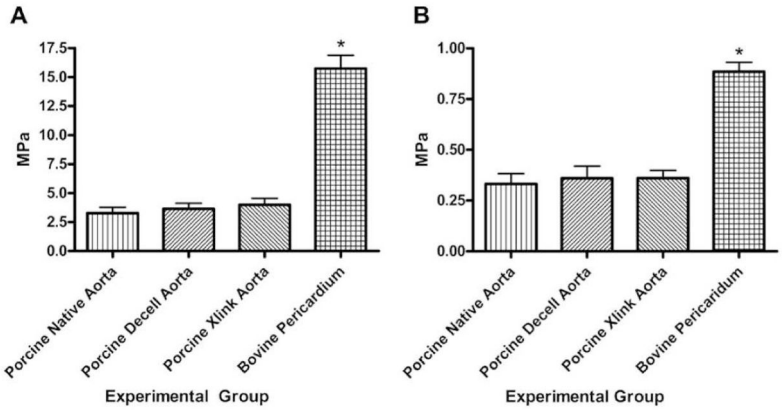

Figure 1.

Suture Pullout testing on porcine and bovine tissues. a) Modulus of elasticity of the patch materials; b) Tensile stress at maximum load. The asterisk denotes a significantly higher values for the bovine pericardium patch than the porcine experimental groups.

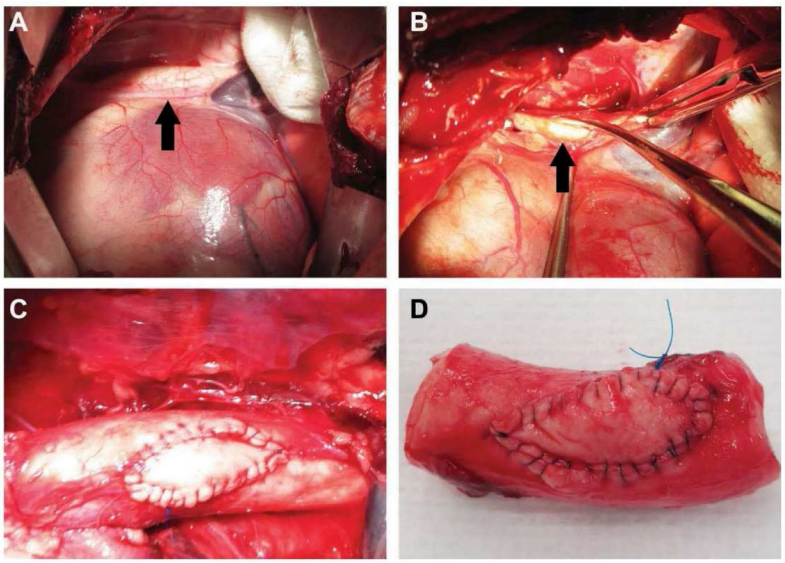

Figure 2.

Implantation of the patch material on the thoracic aorta. a) Access to the thoracic aorta (black arrow) was done through the 5th and 6th rib space; b) The aorta was isolated and partially clamped before a defect (black arrow) was made into the lumen; c) The material *in vivo* just after implantation; d) The material explanted less than 3 hours post implantation (non-survival animal).

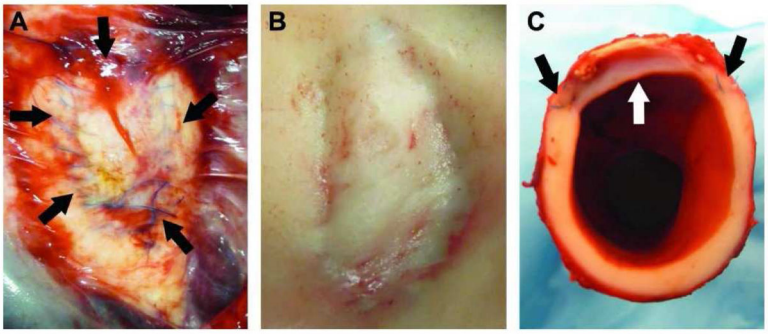

Figure 3.

Thoracic aorta patched with the biomaterial after 6 months of implantation. a) The patch still in vivo. The suture material can still be seen on the adventitial layer of the vessel. There is minimal scar tissue such that the patch is visible through it. The arrows indicate the outline of the patch; b) The lumen of the aorta with the patch. There are no blood clots associated with the patch and grossly it has integrated smoothly with the host tissue; c) A cross sectional view of the aorta through the patch showing the smooth transition between patch and native tissue.

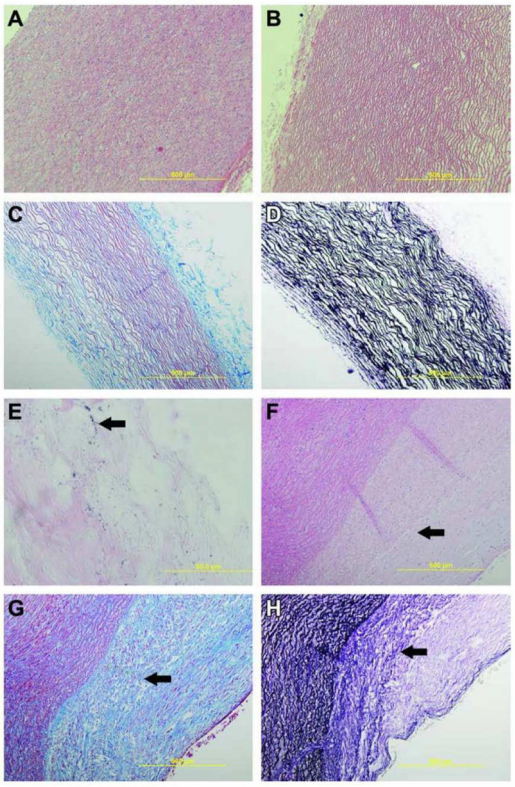

Figure 4.

Histology of native control tissue and pristine biomaterial. a) 100× H&E staining of native porcine aorta with cell nuclei present; b) 100× H&E staining of decellularized aorta showing removal of cellular components; c) 100× Masson's trichrome staining of the biomaterial with a black arrow indicating collagen and the white arrow indicating lighter staining collagen; d) 100× van Geison's stain of the biomaterial showing the presence of the black elastin fibers; e) 1000× H&E staining of the biomaterial showing the presence of the AuNPs; f) 100× H&E staining of native tissue and the biomaterial at 6 months. Arrow indicates the nuclei of cells that have moved into the patch area; g) 100× Masson's trichrome staining of the biomaterial with a black arrow indicating the transition zone between the biomaterial and native tissue; h) 100× van Geison's stain of the biomaterial showing the presence of the black elastin fibers. The black arrow indicates that the transition zone where the biomaterial patch is presenting characteristics more similar to the native tissue.

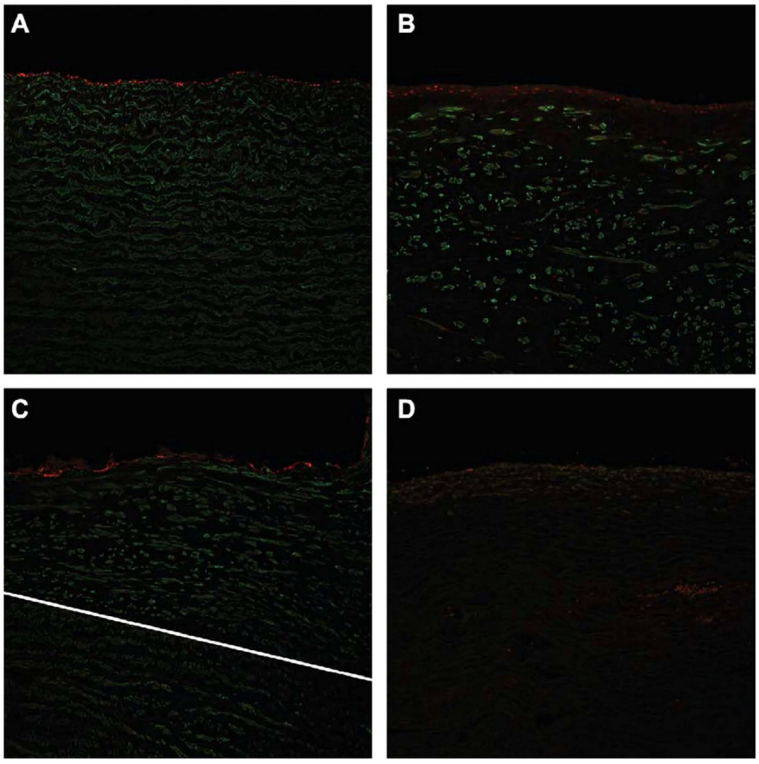

Figure 5.

Immunohistochemical staining of endothelial (red) and SMCs (green) taken at 200x. a) Native aortic tissue taken from a control animal (no surgical intervention). There is a smooth line of endothelial cells present on the lumen of the vessel with typical SMC patterning below it. b) The nanocomposite biomaterial 6 months after implantation showing a smooth, single layer of endothelial cells (red) comparable to the control tissue. There are also SMCs present throughout the area below the endothelial cells. c) The white line indicates the transition between native tissue and the implanted biomaterial. The SMCs have integrated the biomaterial and are forming patterns much like the native tissue. There is a smooth layer of endothelial cells present on the luminal side. d) This image is of a patch that was implanted less than 2 hours. It shows a lack of SMCs or endothelial cell growth, indicating what is present in the other images is not autofluorescence, but evidence of true cellular integration and remodeling.